Relativistic magnetohydrodynamic simulations of astrophysical plasmas

Luca Del Zanna

Dipartimento di Fisica e Astronomia, Università degli Studi di Firenze

INAF - Osservatorio Astrofisico di Arcetri

INFN - Sezione di Firenze

luca.delzanna@unifi.it

Relativistic Hydrodynamics, MITP, October 2016 - Mainz

Outline

From relativistic hydrodynamics to MHD

Plasmas in space and solar environments

The baryonic component in the Universe is almost invariably found in the *fourth state* of matter: a plasma, ionized gas where magnetic fields and currents play a crucial role.

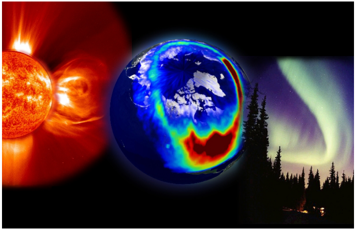

The solar corona is threaded by magnetic fields (active regions above Sun spots, loops, prominences), a continuous supersonic and magnetized outflow fills the whole heliosphere (the solar wind), interacting with the magnetospheres of planets (aurorae).

Plasma physics is non-relativistic in space and solar environments, either treated kinetically (non-Maxwellian distributions, PIC or hybrid codes), or with a macroscopic fluid approach: magnetohydrodynamics (MHD).

The interstellar magnetic field

The Plank satellite is able to produce all-sky maps of polarized light, tracing the magnetic fields in the galactic plane, particularly in the denser molecular clouds.

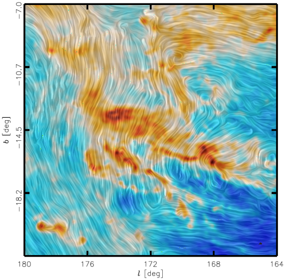

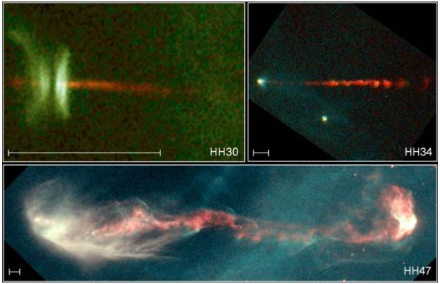

Magnetic field is crucial for star formation: the turbulent MHD additional pressure prevents excessive collapse. Disks and jets threaded and collimated by magnetic fields.

Relativistic plasmas

Strong gravity around compact objects (neutron stars, black holes), high speed velocities, extremely hot temperatures, huge magnetic fields: relativistic plasmas.

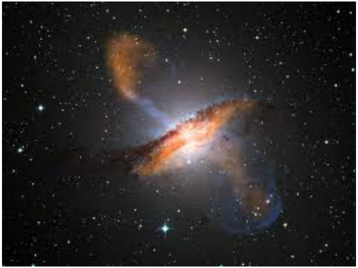

Sources of high-energy astrophysics powered by magnetic fields: pulsars and magnetars, pulsar wind nebulae (PWNe), X-ray binaries, GRBs, AGNs.

These fascinating systems are nowadays investigated by means of numerical simulations in the general relativistic magnetohydrodynamic (GRMHD) regime.

The covariant equations for matter and fields

The equations for general relativistic hydrodynamics are those for baryon number (or equivalently mass) conservation and energy-momentum conservation

$$\nabla_\mu N^\mu = 0,$$
$$\nabla_\mu T^{\mu\nu} = 0,$$

supplemented by the second law of thermodynamics

$$\nabla_\mu \mathcal{S}^\mu \geq 0,$$

where $\mathcal{S}^\mu$ is the entropy current.

In relativistic MHD $T^{\mu\nu}$ is the *total* (matter and fields) energy-momentum tensor of the system, and the above equations are unchanged. The electromagnetic field obeys

$$\nabla_\mu F^{\mu\nu} = -I^\nu, \quad (\nabla_\nu I^\nu = 0)$$
$$\nabla_\mu F^{\star\mu\nu} = 0,$$

where $F^{\mu\nu}$ is the Faraday tensor and $F^{\star\mu\nu} = \frac{1}{2}\epsilon^{\mu\nu\lambda\kappa}F_{\lambda\kappa}$ its dual ($c \to 1, 4\pi \to 1$).

If we split the energy-momentum tensor and introduce the Lorentz force, we find

$$\nabla_\mu T^{\mu\nu}_{\mathrm{m}} = -\nabla_\mu T^{\mu\nu}_{\mathrm{f}} = -I_\mu F^{\mu\nu},$$

where $T^{\mu\nu}_{\mathrm{m}}$ and $T^{\mu\nu}_{\mathrm{f}}$ are the *matter* and *field* contributions, the latter given by

$$T^{\mu\nu}_{\mathrm{f}} = F^{\mu\lambda}F^{\nu}_{\lambda} - \frac{1}{4}g^{\mu\nu}F^{\lambda\kappa}F_{\lambda\kappa}.$$

Decomposition with u^μ and the ideal MHD condition

If dissipative effects are neglected and we introduce the *fluid* velocity u^μ, we have

$$N^\mu = n u^\mu,$$
$$T_{\mathrm{m}}^{\mu\nu} = e u^\mu u^\nu + p\Delta^{\mu\nu} = (e+p)u^\mu u^\nu + p g^{\mu\nu},$$
$$\mathcal{S}^\mu = s u^\mu,$$

where baryon density, energy density, kinetic pressure, and entropy density are

$$n = -N^\mu u_\mu, \quad e = T_{\mathrm{m}}^{\mu\nu} u_\mu u_\nu, \quad p = \tfrac{1}{3}\Delta_{\mu\nu} T_{\mathrm{m}}^{\mu\nu}, \quad s = -\mathcal{S}^\mu u_\mu.$$

The Faraday tensor and its dual can also be split according to u^μ

$$F^{\mu\nu} = u^\mu e^\nu - u^\nu e^\mu + \epsilon^{\mu\nu\lambda\kappa} b_\lambda u_\kappa,$$
$$F^{\star\mu\nu} = u^\mu b^\nu - u^\nu b^\mu - \epsilon^{\mu\nu\lambda\kappa} e_\lambda u_\kappa,$$

where $e^\mu = F^{\mu\nu} u_\nu$ and $b^\mu = F^{\star\mu\nu} u_\nu$ are the electric and magnetic fields in the comoving frame ($e^\mu u_\mu = b^\mu u_\mu = 0$). The ideal MHD condition is

$$e^\mu = 0,$$

that is the comoving electric field vanishes, to prevent huge currents due to the extremely high conductivity of the plasma.

The equations of ideal GRMHD

The field component of $T^{\mu\nu}$ and the dual of the Faraday tensor simplify to

$$
\begin{aligned}
T_{\rm f}^{\mu\nu} &= \tfrac{1}{2}b^2u^\mu u^\nu + \tfrac{1}{2}b^2\Delta^{\mu\nu} - b^\mu b^\nu = b^2u^\mu u^\nu + \tfrac{1}{2}b^2 g^{\mu\nu} - b^\mu b^\nu, \\
F^{\star\mu\nu} &= u^\mu b^\nu - u^\nu b^\mu.
\end{aligned}
$$

The system of ideal GRMHD equations in conservative form is

$$
\begin{aligned}
&\nabla_\mu(\rho u^\mu) = 0, \\
&\nabla_\mu[(e+p+b^2)u^\mu u^\nu + (p+\tfrac{1}{2}b^2)g^{\mu\nu} - b^\mu b^\nu] = 0, \\
&\nabla_\mu(u^\mu b^\nu - u^\nu b^\mu) = 0,
\end{aligned}
$$

in the unknowns $\rho = nm$, e, p, u^μ, b^μ, to be closed with an EoS $p = \mathcal{P}(\rho, e)$.

In the laboratory fixed frame and in a Minkowskian spacetime, we have

$$
u^\mu = (\gamma, \gamma\mathbf{v}), \quad b^\mu = (\gamma(\mathbf{v}\cdot\mathbf{B}), \mathbf{B}/\gamma + \gamma(\mathbf{v}\cdot\mathbf{B})\mathbf{v}), \quad b^2 = B^2/\gamma^2 + (\mathbf{v}\cdot\mathbf{B})^2.
$$

E is now a derived quantity and the sourceless Maxwell equations are for **B** only

$$
\mathbf{E} = -\mathbf{v}\times\mathbf{B}, \qquad \frac{\partial\mathbf{B}}{\partial t} = \boldsymbol{\nabla}\times(\mathbf{v}\times\mathbf{B}), \quad \boldsymbol{\nabla}\cdot\mathbf{B} = 0,
$$

the *induction equation* and the *solenoidal condition*, as in non-relativistic MHD.

The ECHO code for GRMHD

For multi-dimensional simulations of relativistic plasmas the Firenze group developed the shock-capturing Eulerian Conservative High Order code (Del Zanna et al. 2003, 2007), solving the (G)RMHD system of conservation laws (here for a flat metric):

$$\frac{\partial}{\partial t}(\rho\gamma) + \boldsymbol{\nabla}\cdot(\rho\gamma\boldsymbol{v}) = 0,$$

$$\frac{\partial}{\partial t}\left(w\gamma^2\boldsymbol{v} + \boldsymbol{E}\times\boldsymbol{B}\right) + \boldsymbol{\nabla}\cdot\left(w\gamma^2\boldsymbol{v}\boldsymbol{v} - \boldsymbol{E}\boldsymbol{E} + \boldsymbol{B}\boldsymbol{B} + (p + u_{\mathrm{em}})\,\boldsymbol{I}\right) = 0,$$

$$\frac{\partial}{\partial t}\left(w\gamma^2 - p + u_{\mathrm{em}}\right) + \boldsymbol{\nabla}\cdot\left(w\gamma^2\boldsymbol{v} + \boldsymbol{E}\times\boldsymbol{B}\right) = 0,$$

$$\frac{\partial\boldsymbol{B}}{\partial t} + \boldsymbol{\nabla}\cdot(\boldsymbol{v}\boldsymbol{B} - \boldsymbol{B}\boldsymbol{v}) = 0,$$

where $w = e + p$, $u_{\mathrm{em}} = \frac{1}{2}(E^2 + B^2)$ and $\boldsymbol{E} = -\boldsymbol{v}\times\boldsymbol{B}$, $p = \mathcal{P}(\rho, e)$.

Extensions and sub-versions of ECHO (`www.astro.unifi.it/echo/`):

- X-ECHO (Bucciantini & Del Zanna 2011) - GRMHD evolution in a variable spacetime metric (under the *extended* conformally flat condition),
- XNS - equilibrium configurations for magnetized rotating neutron stars,
- ECHO-QGP (Del Zanna et al. 2013; Inghirami et al. 2016) - viscous RHD and ideal RMHD for heavy-ion collisions.

Numerical modeling of pulsars and their environment

Magnetized neutron stars and pulsars

Neutron stars are compact objects ($M \sim 1 - 2M_\odot$, $R \sim 10 - 12$ km), main actors of high-energy astrophysics, nuclear physics, and theoretical physics.

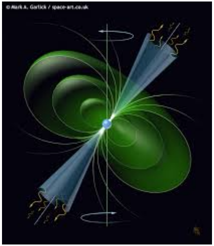

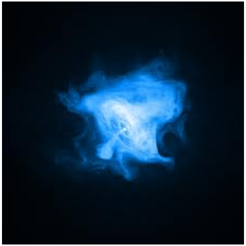

Spindown energy emission due to fast rotation ($P \sim 3 \times 10^{-2} - 3$ s) and strong magnetic fields ($B \sim 10^{11} - 10^{13}$ G) relevant for young objects. Brief history:

- predicted to be the outcome of SN explosions (Baade & Zwicky 1934)
- predicted to produce EM winds powering PWNe (Pacini 1967)
- discovered as radio pulsars (Hewish et al. 1968, now > 2000)
- discovered as gamma-ray emitters (FERMI 2008, now > 150)
- sources of GWs in binary systems (Hulse & Taylor 1975, LIGO/Virgo 2017?)

From pulsars to magnetars

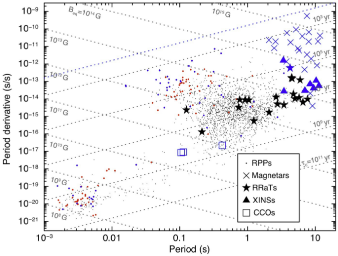

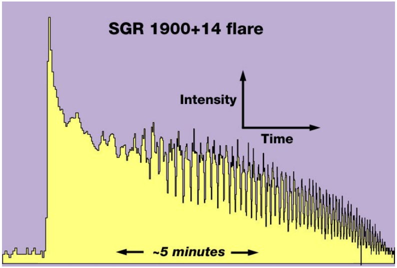

Besides *rotation-powered pulsars* (RPPs) there are other classes of isolated NSs with $B \sim 10^{14} - 10^{15}$ G and longer periods ($P \sim 10$ s), namely magnetars:

- such a high B may form via MHD dynamo during core collapse in a SN event provided initial $P \sim 1 - 3$ ms (Thompson & Duncan 1992),
- irregular X-ray activity (AXPs) and γ-ray flares up to 10^{46} erg (SGRs),
- spindown power inefficient: sporadic release of magnetic energy.

A complex structure of magnetic fields / currents is needed (Turolla et al. 2015).

The millisecond-magnetar model for long and short GRBs

Provided a millisecond magnetar can form during SN core-collapse or after a binary NS merger, spindown driven relativistic winds with $\Gamma \sim \sigma \sim 10^3$ and $\dot{E} \sim 10^{49}$ erg/s are expected (Metzger et al. 2007, 2011, Bucciantini et al. 2012):

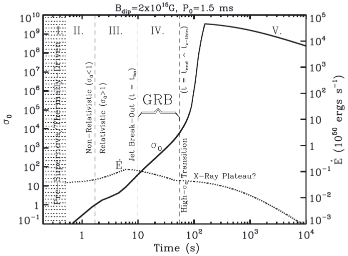

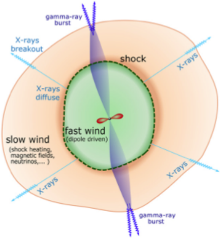

- confinement of the proto-magnetar wind by the external envelopes collimates GRB jets within a hot, magnetized bubble ∼PWN (Bucciantini et al. 2008),
- X-ray plateau (Rowlinson et al. 2010) due to spindown activity (Dall'Osso et al. 2011),
- time-reversal scenario, (Siegel & Ciolfi 2015, Rezzolla & Kumar 2015): hyper-massive magnetar and Kerr-BH could be both involved?
- double GRB events may be explained by quark-deconfinement (Pili et al. 2016).

Axisymmetric FFE and MHD equilibria in GR

The main characters of high-energy astrophysics (PWNe, GRBs, AGNs) are invariably powered by magnetized plasma interacting with rotating NSs/BHs. Modeling requires:

- gravity in the strong regime $\rightarrow$ general relativity,
- magnetic fields in conducting plasmas $\rightarrow$ FFE or MHD,
- rotation $\rightarrow$ frame dragging and/or fluid-like velocities,
- axisymmetry and steady-state $\rightarrow$ reasonable minimal assumptions.

The covariant equations for plasmas in a strong gravitational field are:

$$\nabla_\mu N^\mu = 0, \quad \nabla_\mu T^{\mu\nu}_{\mathrm{m}} = -I_\mu F^{\mu\nu},$$

$$\nabla_\mu F^{\mu\nu} = -I^\nu, \quad \nabla_\mu F^{\star\mu\nu} = 0.$$

- GRMHD: matter and electromagnetic energies are comparable, a main (baryonic) current $N^\mu = nu^\mu$ is defined and the electric field is assumed to vanish in the comoving frame of the fluid: $e^\mu \equiv F^{\mu\nu} u_\nu = 0$.
- Force-Free Electrodynamics: the Lorentz force dominates, the first equation is irrelevant and the second reduces to: $L^\mu \equiv F^{\mu\nu} I_\nu = 0$.

In vacuum, as often assumed in NS magnetospheric modeling, especially for rotating cases, one simply sets $I^\mu = 0$ for numerical convenience.

Stationary and axisymmetric Maxwell's equations

Consider now a stationary and axisymmetric $3+1$ metric with $\partial_t = \partial_\varphi = 0$ in the form

$$ds^2 = -\alpha^2 dt^2 + \gamma_{11}(dx^1)^2 + \gamma_{22}(dx^2)^2 + R^2(d\varphi - \omega dt)^2,$$

where α is the *lapse function*, $\beta = -\omega R \mathbf{e}_{\hat\varphi}$ the *shift vector* (frame dragging velocity), $\gamma_{33} = R^2$. The stationary Maxwell equations are (Thorne & Macdonald 1982)

$$\nabla \times (\alpha \mathbf{E} + \beta \times \mathbf{B}) = 0, \quad \nabla \cdot \mathbf{B} = 0,$$

$$\nabla \times (\alpha \mathbf{B} - \beta \times \mathbf{E}) = \alpha \mathbf{J} - \rho_e \beta, \quad \nabla \cdot \mathbf{E} = \rho_e.$$

From the solenoidal constraint we define the magnetic flux function $\Psi \equiv A_\varphi$ such that

$$\mathbf{B} = \frac{\nabla\Psi}{R} \times \mathbf{e}_{\hat\varphi} + \frac{\mathcal{I}}{\alpha R}\mathbf{e}_{\hat\varphi},$$

and any function f satisfying $\mathbf{B}\cdot\nabla f = 0$ will be constant over magnetic surfaces and $f = f(\Psi)$ alone. The last two Maxwell equations provide the conduction current

$$\mathbf{J} = \frac{\nabla\mathcal{I}}{\alpha R} \times \mathbf{e}_{\hat\varphi} + J_{\hat\varphi}\mathbf{e}_{\hat\varphi}, \qquad \frac{\alpha}{R}J_{\hat\varphi} = -\nabla\cdot\left(\frac{\alpha}{R^2}\nabla\Psi\right) + \mathbf{E}\cdot\nabla\omega,$$

whereas the first Maxwell equation implies $E_\varphi = 0$ and, using $\Phi \equiv A_t$

$$\alpha\mathbf{E} + \beta \times \mathbf{B} = \nabla\Phi \Rightarrow \mathbf{E} = \frac{\nabla\Phi + \omega\nabla\Psi}{\alpha}.$$

FFE case (NS magnetosphere): the Grad-Shafranov equation

If in vacuum, $\rho_e = \mathbf{J} = 0$ and two coupled PDEs for Ψ and Φ are derived.

Inside a highly conducting plasma holds the degenerate condition

$$\mathbf{E} \cdot \mathbf{B} = 0,$$

then $\mathbf{B} \cdot \nabla\Phi = 0 \Rightarrow \Phi = \Phi(\Psi)$ and a *drift velocity* $\mathbf{v}$ can be always defined, such that

$$\mathbf{E} = -\mathbf{v} \times \mathbf{B} = -\frac{v}{R}\nabla\Psi, \quad v \equiv v_{\hat\varphi} = \frac{\Omega - \omega}{\alpha} R, \quad \Omega = -\frac{d\Phi}{d\Psi}.$$

The Lorentz force acting on the plasma is

$$\mathbf{L} = \rho_e \mathbf{E} + \mathbf{J} \times \mathbf{B} = \left(\frac{J_{\hat\varphi}}{R} - \rho_e \frac{v}{R}\right)\nabla\Psi - \frac{\mathcal{I}\,\nabla\mathcal{I}}{\alpha^2 R^2} + \frac{\nabla\mathcal{I} \times \nabla\Psi \cdot \mathbf{e}_{\hat\varphi}}{\alpha R^2}\mathbf{e}_{\hat\varphi},$$

The FFE condition $\mathbf{L} = 0$ implies $\mathcal{I} = \mathcal{I}(\Psi)$ and the Grad-Shafranov equation

$$\nabla \cdot \left[\frac{\alpha}{R^2}\left(1 - v^2\right)\nabla\Psi\right] + \frac{v}{R}\frac{d\Omega}{d\Psi}|\nabla\Psi|^2 + \frac{\mathcal{I}}{\alpha R^2}\frac{d\mathcal{I}}{d\Psi} = 0.$$

a PDE providing the magnetic structure Ψ for given $\mathcal{I}(\Psi)$ and $\Omega(\Psi)$, with extra conditions at the *light cylinder* $v = 1 \Rightarrow R = R_{\mathrm{L}} \equiv \alpha/(\Omega - \omega)$.

The pulsar equation is retrieved in flat space for $\alpha = 1$ and $\Omega = \mathrm{const}$.

GRMHD case (NS interior): the Bernoulli equation

Consider now matter in a NS assuming $\mathbf{v} = v\mathbf{e}_{\hat\varphi}$ and uniform rotation:

$$u^\mu = (\Gamma/\alpha, 0, 0, \Omega\Gamma/\alpha), \quad \Gamma = (1 - v^2)^{-1/2}, \quad \Omega \equiv u^\varphi/u^t = \text{const},$$

where v retains the previous form. The Euler equation, including the Lorentz force is

$$\rho h a_\mu + \partial_\mu p + u_\mu u^\nu \partial_\nu p = L_\mu \Rightarrow \partial_i p - \rho h \partial_i \ln(\Gamma/\alpha) = L_i.$$

If we now make the simplifying assumptions:

- barotropic EoS $p = \mathcal{P}(\rho)$ (e.g. polytropic law): $\quad p = K\rho^{1+1/n}$,
- conservative Lorentz force with potential $\mathcal{M}$: $\quad \mathbf{L} = \rho h \nabla \mathcal{M}$,

the equation can be solved, providing the GRMHD Bernoulli integral

$$\ln(h/h_c) + \ln(\alpha/\alpha_c) - \ln\Gamma = \mathcal{M}.$$

Further compatibility conditions are $\mathcal{I} = \mathcal{I}(\Psi)$, $\mathcal{M} = \mathcal{M}(\Psi)$, and the GS equation is

$$\nabla \cdot \left[\frac{\alpha}{R^2\Gamma^2}\nabla\Psi\right] + \frac{\mathcal{I}}{\alpha R^2}\frac{d\mathcal{I}}{d\Psi} + \alpha\rho h\frac{d\mathcal{M}}{d\Psi} = 0,$$

with the previous case retrieved by simply letting $\rho \to 0$.

Einstein equations in the (X)CFC approximation

The stationary and circular metric is conveniently approximated to the conformally flat form (CFC assumption, e.g. Wilson & Mathews 2003):

$$ds^2 = -\alpha^2 dt^2 + \psi^4[dr^2 + r^2 d\theta^2 + r^2 \sin^2\theta (d\phi - \omega dt)^2],$$

with ψ the *conformal factor*. The Einstein equations simplify to the system

$$\Delta\psi = -[2\pi E + \tfrac{1}{8} K_{ij}K^{ij}]\,\psi^5,$$

$$\Delta(\alpha\psi) = [2\pi(E + 2S) + \tfrac{7}{8} K_{ij}K^{ij}]\,\alpha\psi^5,$$

$$\Delta\omega = -16\pi\alpha\psi^4 S^\phi - 2\psi^{10} K^{\phi j}\partial_j(\alpha\psi^{-6}),$$

where K_{ij} is the *extrinsic curvature*, computed via derivatives of ω, whereas sources E, S, and S^ϕ are determined by the fluid quantities and EM fields.

In the rotating case, a more efficient and very robust method is the *eXtended* CFC approximation (XCFC, Cordero-Carrión 2009, Bucciantini & Del Zanna 2011) allowing for a hierarchical scheme and uniqueness of solution (one extra equation needed).

Numerical models for rotating NS are consistent with full GR within accuracy of 10^{-4}.

XCFC metric also employed in dynamical Einstein+GRMHD evolution: X-ECHO code.

The XNS code

Nonlinear PDEs solved via decomposition in scalar and vector spherical harmonics

$$u(r,\theta) = \sum [A_l(r) Y_l(\theta)], \qquad X_{\hat\phi}(r,\theta) = \sum [C_l(r) Y_l'(\theta)],$$

grid discretization, and direct inversion of tridiagonal matrices.

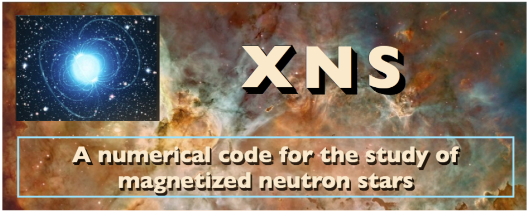

XNS code (www.arcetri.inaf.it/science/ahead/XNS). Iterative scheme:

- provide initial static and radially symmetric guess (TOV equations),
- solve Einstein equations for the XCFC metric $\rightarrow \alpha, \psi, \omega$,
- solve Maxwell equations (or GS) for EM fields $\rightarrow \Psi, \Phi \rightarrow \mathbf{B}, \mathbf{E}$,
- solve Bernoulli integral for matter (polytropic or tabulated EoS) $\rightarrow \rho, p, \mathbf{v}$.

Purely toroidal fields

For purely toroidal fields $\Psi = 0$ and we need $\mathcal{M} = \mathcal{M}(\mathcal{I})$, a solution is ($m \geq 1$):

$$\nabla\mathcal{I} + \alpha^2 R^2 \rho h \nabla\mathcal{M} = 0, \quad \mathcal{I} = \alpha R B_{\hat{\phi}} = K_m(\alpha^2 R^2 \rho h)^m.$$

The Lorentz force produces axial compression, providing prolate static configurations.
For increasing m the field is confined to a narrow torus farther from the axis.

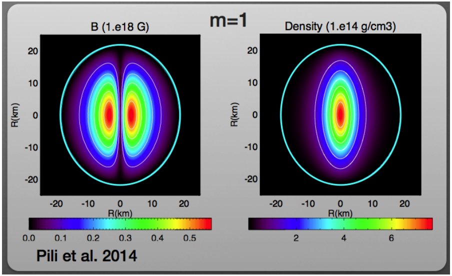

If an NS with eccentricity $\bar{e} = 1 - I_{xx}/I_{zz} \sim 10^{-3}$ is born with initial slight tilt and later orthogonalize, GWs will be detectable (Dall'Osso et al. 2009). For $B_{\rm max} \leq 10^{17}\,\rm G$ we find:

$$\bar{e} \simeq -9 \times 10^{-3}(B_{\rm max}/10^{17}\,\rm G)^2 + 3 \times 10^{-3}(P/10\,\rm ms)^{-2}.$$

Purely poloidal fields

The free functions for GS are chosen as (Pili et al. 2014, Bucciantini et al. 2015):

$$\mathcal{M}(\Psi) \propto \Psi[1 + \xi \tfrac{1}{\nu+1}(\Psi/\Psi_{\max})^{\nu}], \qquad \mathcal{I}(\Psi) \propto \tfrac{1}{\zeta+1}(\Psi/\Psi_{\max} - 1)^{\zeta+1},$$

providing currents confined inside the NS. Here $\mathcal{I} = 0$ for purely poloidal fields.

Magnetosphere calculated self-consistently (FFE if static, vacuum in the rotating case).

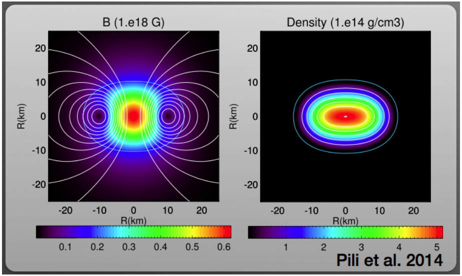

Global eccentricity always positive (oblate configurations), increasing with rotation

$$\bar{e} \simeq 5 \times 10^{-3}(B_{\max}/10^{17}\,\mathrm{G})^2 + 3 \times 10^{-3}(P/10\,\mathrm{ms})^{-2}.$$

Structure of electrosphere in rotating stars

In the uniformly rotating case $\Omega = \mathrm{const}$, inside the NS holds the MHD condition

$$\Phi = -\Omega\Psi + C,$$

whereas Φ is independent in the vacuum magnetosphere (continuity is enforced).

The constant C is determined by either imposing (Pili et al. *in prep.*):

- vanishing net charge of NS (extraction of e^- from polar caps),
- vanishing electric field at poles (NS is globally charged).

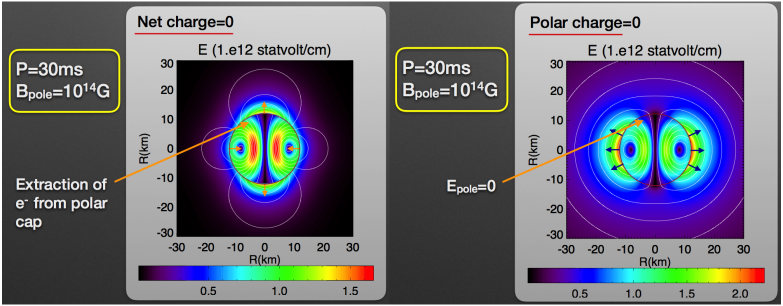

Twisted-torus configurations

Twisted-torus mixed configurations required for stability, different current distributions attempted all provide a too small value $\mathcal{H}_{\rm tor}/\mathcal{H}_{\rm tot} \leq 10\%$ (Bucciantini et al. 2015), contrary to previous studies where $\mathcal{H}_{\rm tor}/\mathcal{H}_{\rm tot} \leq 90\%$ (Ciolfi & Rezzolla 2013).

Twist angle increases with $B_{\rm tor}/B_{\rm pol}$, saturating at ~ 2 rad (self-regulation).

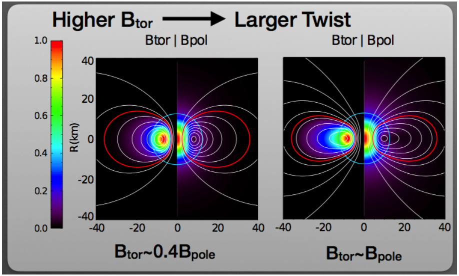

The presence of magnetospheric currents comparable to the internal ones leads to a change in fieldlines topology and to plasmoid-like (unstable) solutions.

Poloidal field always dominant, global eccentricity positive (oblate configurations).

Application: quark deconfinement and double-peaked GRBs

The two-families scenario of Hadronic Stars and Quark Stars (Drago et al. 2014, 2016, Bombaci et al. 2016) may match observations, provided strangeness enters the EoS.

The spindown evolution equation is solved on top of XNS rotating equilibria models, providing tracks in $M - \rho_c$ or $M - R$ diagrams (Pili et al. 2016). The scenario is:

- a HS ms-magnetar (in the yellow region) produces a first GRB,
- large spindown leads to increase of ρ_c and quark deconfinement ($M_0, J = \mathrm{const}$),
- the new ms-magnetar, in the QS branch, produces a second event.

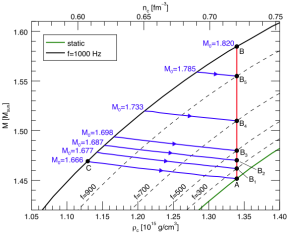

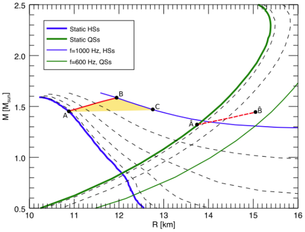

A *model* for the double-event GRB110709B. An initial HS with

$$B \simeq 2 \times 10^{15} G, \quad M_0 \simeq 1.7 M_\odot, \quad P \simeq 1 - 1.5 ms$$

provides the correct energetics of both bursts and characteristic timescales.

Pulsar winds and nebulae

The spindown energy losses from a young pulsar drive a relativistic plasma wind made of pairs and (mainly toroidal) magnetic fields, after light cylinder magnetization $\sigma \gg 1$.

Impact with expanding SN ejecta creates the PWN (e.g. the Crab Nebula) shining in synchrotron light from radio to γ-rays (Rees & Gunn 1974; Kennel & Coroniti 1984).

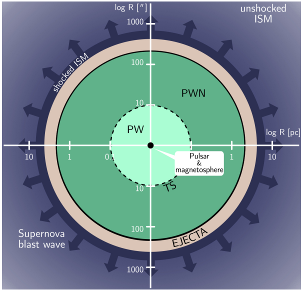

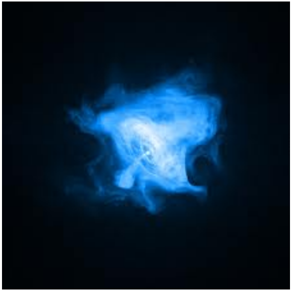

The millennium challenge from Chandra to theorists: can you explain all that?!?

Multidimensional relativistic MHD simulations are powerful tools to investigate the properties of pulsar winds (magnetization, anisotropy, composition).

Formation of the polar jets

A jet/torus structure as observed in X-rays needs two ingredients (Lyubarsky 2002):

- an axisymmetric anisotropic pulsar wind (stronger equatorial flux $\rightarrow$ oblate TS);
- a moderate magnetization $\sigma \sim 1-5\%$ at termination shock (10 times than in 1D).

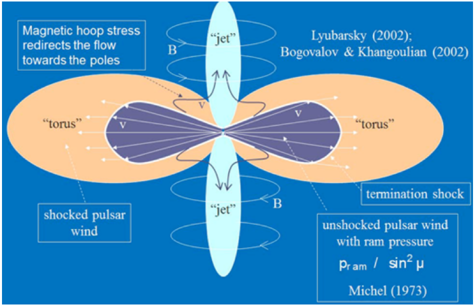

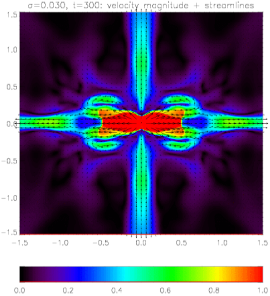

Indeed, in axisymmetric relativistic MHD simulations polar jets form due to *post-shock* magnetic hoop stresses (Komissarov & Lyubarsky 2003/4, Del Zanna et al. 2004).

No prescriptions needed for PWN: self-consistently computed by the numerical code!

Torus, jets, rings, wisps, knots, ...

Simulated synchrotron maps from 2D axisymmetric relativistic MHD computations (here from our ECHO code): with little fine tuning of parameters, the challenge is won!

Detailed recipes, including boosting, polarization, IC, in (Del Zanna et al. 2006; Volpi 2008).

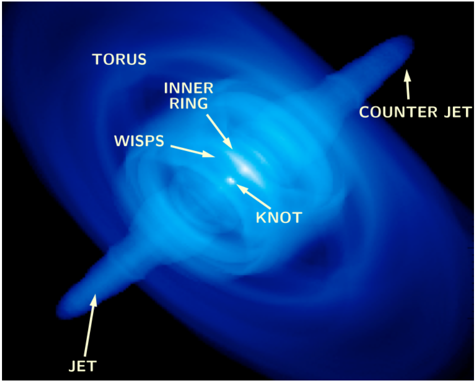

Wisps as probes for acceleration mechanisms

Wisp-like motions with $v/c \sim 0.1 - 0.4$ due to turbulent advection beyond TS with periods $P \simeq 1 - 2$ yr (Volpi et al. 2008; Camus et al. 2009; Olmi et al. 2014).

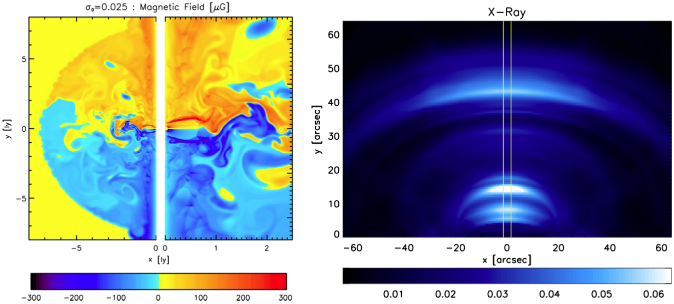

Detailed characterization of single wisps at various frequencies (Olmi et al. 2015):

- radio population with $f_R(\epsilon) \propto \epsilon^{-p_R}$ and $p_R \simeq 1.5$ uniform (reconnection? High σ)
- X-ray population injected in a narrow equatorial belt at TS with $f_X(\epsilon) \propto \epsilon^{-p_X}$ and $p_X > 2$ (Fermi I process? Low σ, as in striped equatorial wind)

3D dynamics: velocity and magnetic fields

3D-AMR simulations (see also Porth et al. 2014) with the PLUTO code aimed at:

- allowing extra degrees of freedom for B, kink instabilities and magnetic dissipation,
- reaching realistic evolution times, at least the self-similar expansion phase,
- reproducing the jet-torus structure and all the detailed features as in 2D,
- finally obtaining the full sync+IC SED without any ad-hoc hypotheses.

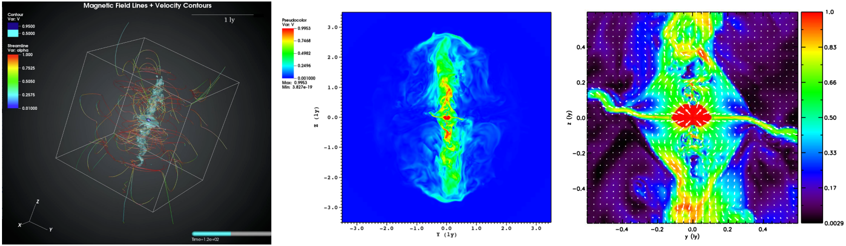

- magnetic/kinetic flux equipartition just before the TS ($\sigma = 1$),
- very strong jet collimation by hoop stresses (here striped wind is narrow),
- B strong in the inner part, where toroidal field dominates, poloidal field in jets.

3D results: surface brightness maps

Surface brightness maps from 3D simulations, radio and X-rays (here in log scale):

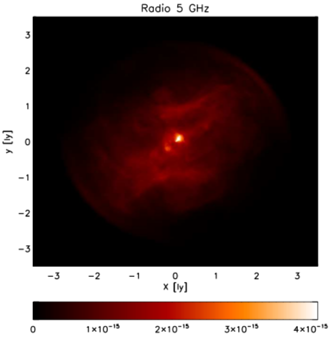

First results in (Olmi et al. 2016), additional simulations with larger striped wind region are ongoing (brighter torus? SED matched?).

Future: inclusion of test particles for a better modeling of emission.

Magnetic dissipation in relativistic plasmas

Reconnection in solar, space, and laboratory plasmas

Magnetic reconnection is a rearrangement of magnetic topology in conducting plasmas with *finite* resistivity. It is the most efficient way to convert the energy of a magnetically dominated plasma into heat and particle acceleration.

Energy release is typically violent and occurs on very rapid timescales.

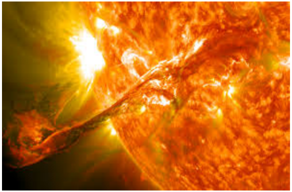

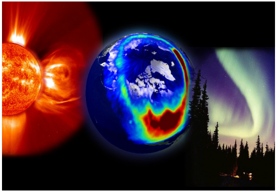

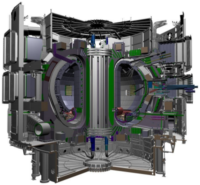

In the solar-terrestrial environment it is responsible for solar flares and geomagnetic storms (thus crucial for space weather).

It is also important in laboratory and fusion reactors (tokamaks: ITER), causing sawtooth instabilities and eventually collapse of core temperature.

Reconnection in relativistic plasmas

In astrophysical sources it may explain several high-energy phenomena:

- the SGR events of magnetars (Lyutikov 2003; Elenbaas et al. 2016)
- jet launching in AGN/microquasar systems (Romanova & Lovelace 1992)
- jet launching in GRB engines (Drenkhahn & Spruit 2002)
- energy conversion in pulsar winds (Coroniti 1990, Sironi & Spitkovsky 2011)
- gamma-ray flares observed in the Crab Nebula (Cerutti et al. 2013, 2014)

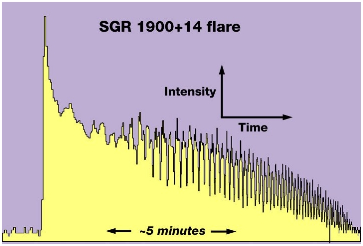

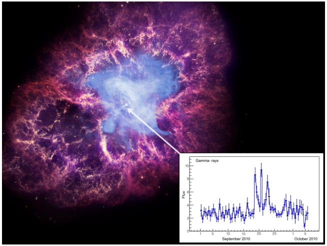

Basic theory: steady-state, driven reconnection (SP model)

Within classical resistive MHD the magnetic field evolution is governed by the induction equation (flux freezing in ideal MHD with $\eta = 0$):

$$\boxed{\frac{\partial \vec{B}}{\partial t} = \nabla \times (\vec{v} \times \vec{B}) + \eta \nabla^2 \vec{B}}$$

Fluid advection and Ohmic diffusion occur on very different timescales:

$$\tau_A = \frac{L}{v_A}, \quad \tau_D = \frac{L^2}{\eta}, \quad S = \frac{L\, v_A}{\eta} = \frac{\tau_D}{\tau_A} \gg 1$$

where S is the Lundquist number, defined on the Alfvén speed v_A.

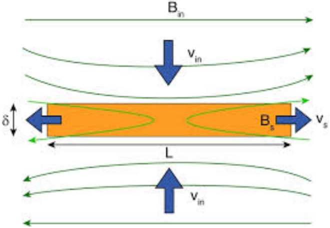

The steady, incompressible Sweet-Parker (1957) model predicts a rate of reconnected flux

$$R = \frac{v_{\rm in}}{v_A} = \frac{\delta}{L} \sim S^{-1/2}$$

leading to time scales $\tau/\tau_A \sim S^{1/2}$, far too slow to explain solar flares ($\tau \sim \tau_A \sim 10^3$s, $S > 10^{12}$).

Basic theory: spontaneous reconnection (tearing mode)

The linear stability of current sheets was investigated by Furth et al. (1963); Coppi et al. (1976). In resistive MHD the equilibrium is unstable to the *tearing mode* leading to the formation of X-points and plasmoids.

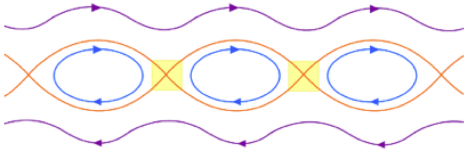

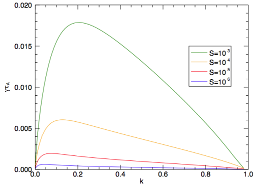

If measured on top of the only available scale, the sheet width a, the instability growth rate $\gamma = 1/\tau$ is, again, far too slow

$$\boxed{\gamma\,\bar{\tau}_A \sim \bar{S}^{-1/2}}\,, \quad k_{\max} a \sim \bar{S}^{-1/4} \quad (\bar{\tau}_A = a/v_A, \quad \bar{S} = a\,v_A/\eta)$$

This is the same scaling of SP, so once more we would need extremely small scales to explain the observations. Sub-MHD Hall/kinetic effects?

Tearing instability of a SP sheet (plasmoid instability)

Revival of one-fluid resistive MHD: discovery of the *plasmoid instability* or *super-tearing* of a SP current sheet (Loureiro et al. 2007; Lapenta 2008; Samtaney et al. 2009; Bhattacharjee et al. 2009; Cassak et al. 2009; Huang & Bhattacharjee 2010).

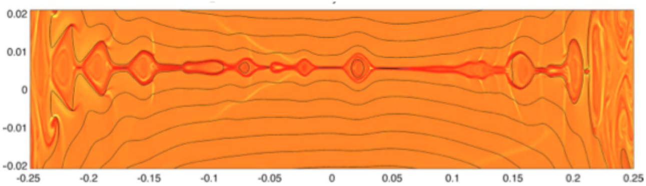

Basically, if we apply the tearing mode to the SP current sheet with $a \equiv \delta = LS^{-1/2}$ and normalize with the *macroscopic* τ_A and L, we find

$$\gamma\,\tau_A \sim S^{1/4} \gg 1, \quad k_{\max} L \sim S^{3/8} \gg 1$$

(for $S > S_c \sim 10^4$) which is clearly a PARADOX!

Also relativistic resistive MHD simulations basically confirmed the same scenario (Watanabe & Yokoyama 2006; Zenitani et al. 2010; Takahashi et al. 2013, Takamoto 2013), with a higher S_c according to simulations with Galerkin methods by Zanotti & Dumbser (2011).

The *ideal* tearing instability

For a generic dependence of the aspect ratio with S, the growth rate is

$$a/L \sim S^{-\alpha} \Rightarrow \gamma \sim \bar{\tau}_A^{-1} \bar{S}^{-1/2} = \tau_A^{-1} S^{-1/2} S^{3/2\alpha}$$

thus, there is a critical value for an *ideal* tearing mode:

$$\boxed{\alpha = 1/3 \Rightarrow \gamma \sim \tau_A^{-1}}$$

For $S = 10^{12}$ the threshold $a/L \sim S^{-1/3} = 10^4$ is 100 times larger than the SP one. Thus reconnection occurs on *ideal* timescales and the SP configuration cannot be realized in nature (Pucci & Velli, 2014).

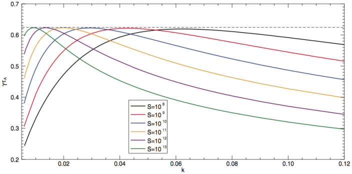

The dispersion relation $\gamma(k)$ for varying S clearly shows an ideal limit

$$\boxed{\gamma_{\max} \simeq 0.63\, \tau_A^{-1}}, \quad k_{\max} a \simeq 1.4\, S^{-1/6}, \quad S \gg 1$$

Simulations (Landi et al. 2015; Tenerani et al. 2015) have fully confirmed this scenario.

Resistivity in the relativistic MHD case

For high-energy astrophysics applications, consider now a relativistic plasma where

$$\sigma = B^2/\rho \sim 1, \qquad \beta = 2p/B^2 \sim 1.$$

The conservative form of resistive relativistic MHD in Minkowski spacetime is

$$\begin{aligned}
&\partial_t(\rho\Gamma) + \boldsymbol{\nabla}\cdot(\rho\Gamma\boldsymbol{v}) = 0 \\
&\partial_t(w\Gamma^2\boldsymbol{v} + \boldsymbol{E}\times\boldsymbol{B}) + \boldsymbol{\nabla}\cdot(w\Gamma^2\boldsymbol{v}\boldsymbol{v} - \boldsymbol{E}\boldsymbol{E} - \boldsymbol{B}\boldsymbol{B} + (p + u_{\rm em})\boldsymbol{I}) = 0 \\
&\partial_t(w\Gamma^2 - p + u_{\rm em}) + \boldsymbol{\nabla}\cdot(w\Gamma^2\boldsymbol{v} + \boldsymbol{E}\times\boldsymbol{B}) = 0 \\
&\partial_t\boldsymbol{B} + \boldsymbol{\nabla}\times\boldsymbol{E} = 0 \\
&\partial_t\boldsymbol{E} - \boldsymbol{\nabla}\times\boldsymbol{B} = -\boldsymbol{J}
\end{aligned}$$

with $\Gamma = 1/\sqrt{1-v^2}$, $w = e + p$, $u_{\rm em} = \frac{1}{2}(E^2 + B^2)$, $p = \mathcal{P}(\rho, e)$. The electric field is not simply provided by $\boldsymbol{E} + \boldsymbol{v}\times\boldsymbol{B} = 0$ but in the resistive case must be evolved by Maxwell's equations, with the eletric current provided by the relativistic Ohm law

$$\boldsymbol{J} = q\boldsymbol{v} + \eta^{-1}\,\Gamma[\boldsymbol{E} + \boldsymbol{v}\times\boldsymbol{B} - (\boldsymbol{E}\cdot\boldsymbol{v})\boldsymbol{v}],$$

for isotropic resistivity, where $q = \boldsymbol{\nabla}\cdot\boldsymbol{E}$. This can be derived from the covariant form:

$$e^\mu = \eta j^\mu, \quad j^\mu \equiv I^\mu - q_0 u^\mu = (q - q_0\Gamma, \boldsymbol{J} - q_0\Gamma\boldsymbol{v}), \quad (q_0 = -I^\mu u_\mu).$$

IMEX (IMplicit-EXplicit) Runge-Kutta high-order methods to treat *stiff* terms $\propto \eta^{-1}$ employed in the ECHO code (Del Zanna et al. 2007, 2014).

The tearing instability in relativistic MHD: linear analysis

We consider 2D, incompressible, linear perturbations of force-free current sheet

$$\boldsymbol{B}_0 = B_0[\tanh(x/a)\hat{\mathbf{y}} + \mathrm{sech}(x/a)\hat{\mathbf{z}}]$$

and retrieve exactly the same equations of the classical MHD with the only exception $\rho_0 \rightarrow w_0 + B_0^2$ as the plasma inertial term (Del Zanna et al. 2016):

$$\partial_t \boldsymbol{B}_1 = \boldsymbol{\nabla} \times (\boldsymbol{v}_1 \times \boldsymbol{B}_0) + \eta \boldsymbol{\nabla}^2 \boldsymbol{B}_1,$$
$$\partial_t (w_0 \boldsymbol{v}_1 + \boldsymbol{E}_1 \times \boldsymbol{B}_0) = -\boldsymbol{\nabla}(p_1 + \boldsymbol{B}_0 \cdot \boldsymbol{B}_1) + (\boldsymbol{B}_0 \cdot \boldsymbol{\nabla})\boldsymbol{B}_1 + (\boldsymbol{B}_1 \cdot \boldsymbol{\nabla})\boldsymbol{B}_0,$$

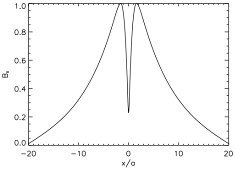

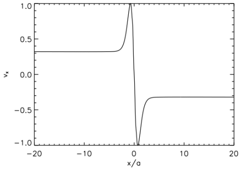

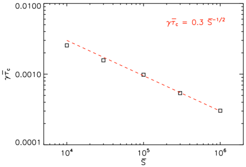

The maximum growth rate then depends of the relativistic Alfvén speed as

$$\gamma_{\max}\bar{\tau}_c \simeq 0.6\, c_A\, \bar{S}^{-1/2}, \quad c_A = B_0/\sqrt{w_0 + B_0^2} = 0.5 \quad (\sigma_0 = \beta_0 = 1)$$

where $\bar{\tau}_c = a/c$ and $\bar{S} = ac_A/\eta$, here from 10^4 to 10^6. Generalization to high S and to relativistic MHD of FFE results (Komissarov et al. 2007).

The *ideal* tearing instability in relativistic MHD

Let us study the tearing instability for the critical (inverse) aspect ratio

$$a/L = S^{-1/3} = 0.01, \quad S = Lc_A/\eta = 10^6$$

Single-mode runs show a clear linear phase and the predicted dispersion relation.

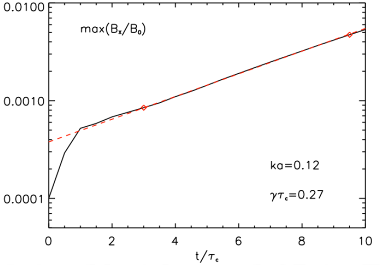

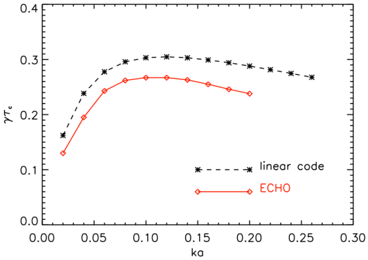

We thus find that the *ideal* tearing mode effectively grows, independently on S, as

$$\boxed{\gamma_{\max} \simeq 0.6c_A/L \sim c/L},$$

that is on light-crossing timescales.

The fully nonlinear case

In our recent paper (Del Zanna et al. 2016) not only the linear phase is described analytically and numerically, but also the subsequent evolution.

In the fully nonlinear and multi-mode case secondary reconnection events occur and the initial ~ 5 islands of the tearing instability start to merge.

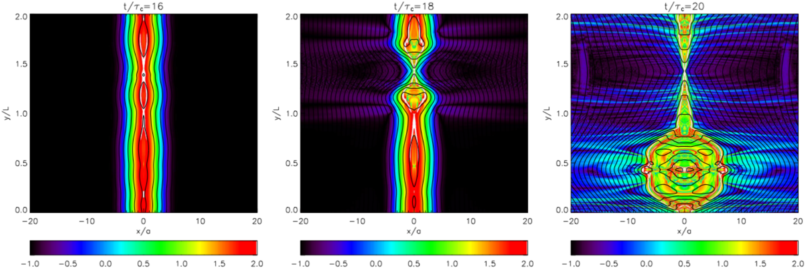

Colors refer to to $|\nabla \times \boldsymbol{B}|$ in log scale. The final evolution is very rapid and we end up with an X-point, two symmetric exhausts, and a major plasmoid where additional instabilities occur (the plasmoid instability is hidden by periodical boundaries).

MHD shocks and Petschek fast reconnection

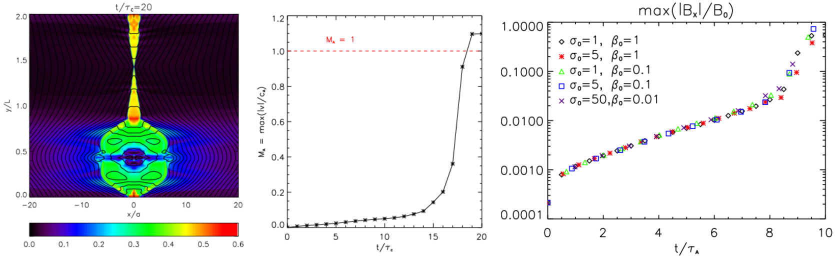

We find a quasi-stationary Petschek scenario for relativistic plasmas (Lyubarsky 2005):

- channels delimited by slow shocks originating from the X-point,
- fast magnetosonic jets propagating in the exhausts and feeding the plasmoid,
- maximum velocity in funnels does not exceed the external c_A (here 0.5),
- we measure $\mathcal{R} \simeq 0.05 - 0.06$, matching the expected fast reconnection rate:

$$\mathcal{R} \equiv M_A = \frac{|v_x|}{c_A} = \frac{\pi}{4 \ln S},$$

- universal growth of perturbations for various σ_0 and β_0, up to $c_A = 0.98$.

Application to magnetars giant flares

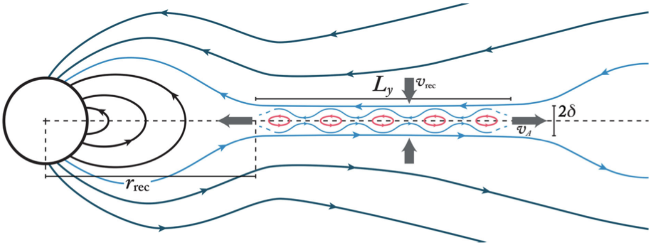

The (standard) tearing instability in current sheets above large coronal loops has been recently employed to model giant flares (SGRs) in magnetars (Elenbaas et al. 2016).

The observed e-folding and peak times in the gamma-ray light curves are

$$\tau_{\rm e} \sim 0.1 - 1\,{\rm ms}, \quad \tau_{\rm peak} \sim 1 - 10\,{\rm ms}$$

Our model for fast reconnection predicts, *independently on S* (thus on microphysics!):

$$\tau_{\rm e} \simeq \frac{1}{\gamma_{\rm max}} \simeq \frac{L}{0.6 c_A} \simeq 0.2\,{\rm ms}, \quad (L \simeq 5 R_\star = 50\,{\rm km},\ c_A \simeq c)$$

provided a thinning process has shrunk the current sheet down to $\delta/L \sim S^{-1/3}$. A similar mechanism may operate at Crab Nebula's termination shock (Olmi et al. 2016).

Summary

In this presentation I have shown theory and numerical applications of the physical regimes typically employed for the modeling of relativistic plasmas in astrophysics.

- In the *ideal case*, the relativistic MHD condition is that of a vanishing electric field in the frame comoving with the fluid, to be used in the evolution equations:

$$e^\mu = 0 \Rightarrow \boldsymbol{E} = -\boldsymbol{v} \times \boldsymbol{B};$$

- When magnetic forces are dominant, the Lorentz force must be balanced as:

$$L^\mu = F^{\mu\nu} I_\nu = 0,$$

  characterizing the *force-free electrodynamics*, or *magnetodynamics*, regime;
- We have used pulsars (magnetars) and their environment as an astrophysical laboratory for relativistic plasmas, where both regimes apply;
- In the *dissipative case*, the primary ingredient used in astrophysics is typically a non-zero *resistivity* η, rather than viscosity. In this case Ohm's law is

$$e^\mu = \eta j^\mu \Rightarrow \boldsymbol{J} = (\nabla \cdot \boldsymbol{E})\boldsymbol{v} + \eta^{-1}\,\Gamma[\boldsymbol{E} + \boldsymbol{v} \times \boldsymbol{B} - (\boldsymbol{E} \cdot \boldsymbol{v})\boldsymbol{v}];$$

- Numerical simulation of fast reconnection in thin current sheets used to model sudden high-energy emission observed in magnetically dominated plasmas, e.g. in magnetars (SGRs) and in pulsar wind nebulae (γ-ray flares in the Crab Nebula).

Thank you!

Summary

In this presentation I have shown theory and numerical applications of the physical regimes typically employed for the modeling of relativistic plasmas in astrophysics.

- In the *ideal case*, the relativistic MHD condition is that of a vanishing electric field in the frame comoving with the fluid, to be used in the evolution equations:

$$e^\mu = 0 \Rightarrow \boldsymbol{E} = -\boldsymbol{v} \times \boldsymbol{B};$$

- When magnetic forces are dominant, the Lorentz force must be balanced as:

$$L^\mu = F^{\mu\nu} I_\nu = 0,$$

  characterizing the *force-free electrodynamics*, or *magnetodynamics*, regime;
- We have used pulsars (magnetars) and their environment as an astrophysical laboratory for relativistic plasmas, where both regimes apply;
- In the *dissipative case*, the primary ingredient used in astrophysics is typically a non-zero *resistivity* η, rather than viscosity. In this case Ohm's law is

$$e^\mu = \eta j^\mu \Rightarrow \boldsymbol{J} = (\nabla \cdot \boldsymbol{E})\boldsymbol{v} + \eta^{-1}\,\Gamma[\boldsymbol{E} + \boldsymbol{v} \times \boldsymbol{B} - (\boldsymbol{E} \cdot \boldsymbol{v})\boldsymbol{v}];$$

- Numerical simulation of fast reconnection in thin current sheets used to model sudden high-energy emission observed in magnetically dominated plasmas, e.g. in magnetars (SGRs) and in pulsar wind nebulae (γ-ray flares in the Crab Nebula).

Thank you!